

Influence of polarity and hydroxyl termination on the band bending at ZnO surfaces

R. Heinhold,¹ G. T. Williams,² S. P. Coolil,³ D. A. Evans,³ and M. W. Allen^{1,*}

¹*The MacDiarmid Institute for Advanced Materials and Nanotechnology, University of Canterbury, Christchurch 8043, New Zealand*

²*Element Six Limited, Global Innovation Centre, Didcot, OX11 0QR, United Kingdom*

³*Department of Mathematics and Physics, Aberystwyth University, Aberystwyth SY23 3BZ, United Kingdom*

(Received 4 October 2013; revised manuscript received 26 November 2013; published 30 December 2013)

Surface sensitive synchrotron x-ray photoelectron spectroscopy (XPS) and real-time *in situ* XPS were used to study the thermal stability of the hydroxyl termination and downward band bending on the polar surfaces of ZnO single crystals. On the O-polar face, the position of the Fermi level could be reversibly cycled between the conduction band and the band gap over an energetic distance of approximately 0.8 eV ($\sim 1/4$ of the band gap) by controlling the surface H coverage using simple ultrahigh vacuum (UHV) heat treatments up to 750 °C, dosing with H₂O/H₂ and atmospheric exposure. A metallic to semiconductorlike transition in the electronic nature of the O-polar face was observed at an H coverage of approximately 0.9 monolayers. For H coverage less than this, semiconducting (depleted) O-polar surfaces were created that were reasonably stable in UHV conditions. In contrast, the downward band bending on the Zn-polar face was significantly more resilient, and depleted surfaces could not be prepared by heat treatment alone.

DOI: [10.1103/PhysRevB.88.235315](https://doi.org/10.1103/PhysRevB.88.235315)

PACS number(s): 73.20.-r, 78.70.En, 81.05.Dz, 82.80.Pv

I. INTRODUCTION

ZnO is an earth-abundant, wide band-gap semiconductor used in a range of applications, such as gas sensing, catalysis, transparent electronics, and ultraviolet photonics.^{1,2} From a fundamental perspective, ZnO has been the subject of much debate concerning the unusual structural and electronic properties of its various crystallographic surfaces.^{3–17} Principal among these are the competing mechanisms responsible for stabilizing the intrinsic electrostatic instability of its polar surfaces^{3–13} and the accumulation of electrons at the same surfaces in quasi-two-dimensional potential wells.^{14–17} The presence of these surface accumulation layers places ZnO in the company of a small class of *n*-type semiconductors that includes InN, In₂O₃, CdO, and SnO₂, whose near-surface bands bend downward in response to donorlike surface states. These materials are also unusual in that their charge neutrality level (CNL) lies above the conduction band minimum.^{18,19} This unusual CNL position is thought to favor the formation of donorlike surface states and has been used to predict a shallow donor role for hydrogen in these materials.^{18–22}

ZnO is an important test material for investigating the properties of these surface accumulation layers due to the availability of high-quality, free-standing bulk crystals that can be cleaved to provide a variety of polar and nonpolar surfaces.²³ ZnO crystallizes into the wurtzite structure (Fig. 1) characterized by alternate Zn and O atomic planes, arranged in threefold-coordinated double layers separated along the *c* axis by a single Zn-O bond. Cleaving the lattice perpendicular to the *c* axis results in two polar surfaces—the Zn-polar [ZnO(0001)] and the O-polar [ZnO(000 $\bar{1}$)] faces that are bulk terminated by entire outer plans of hexagonally arranged Zn and O atoms, respectively.²⁴ Due to the high electron affinity of oxygen, the Zn-O bond lies at the borderline of ionic and covalent classification,¹ and this is reflected in the literature debate concerning the stability of these polar surfaces. From an ionic point of view, the bulk-terminated Zn-polar and O-polar faces are unstable Tasker-type-3 surfaces characterized by a diverging electrostatic energy,^{25,26} while from a covalent

bonding perspective, each surface zinc (oxygen) atom possesses a partially occupied dangling bond filled with 1/2 (3/2) electrons^{10,27,28} (Fig. 1) that violates the electron counting rule (ECR) for stable semiconducting surfaces.^{29–32}

Since polar ZnO surfaces are common in nature, there is much debate concerning the relative roles of a number of proposed stabilization mechanisms, such as (i) a fractional negative charge transfer from the O-polar to the Zn-polar face,¹¹ (ii) reconstructions that modify the stoichiometry of the polar faces by removing up to 25% of the surface atoms,^{5,9} and (iii) hydroxylation of the bulk-terminated surfaces via the adsorption of OH groups on the Zn-polar face and H on the O-polar face.⁶ In recent years, mechanisms (ii) and (iii) have gained increasing support following the discovery by Dulub *et al.*^{5,6} of triangular-shaped pit and terrace reconstructions on sputter-cleaned Zn-polar surfaces and the widely reported observation of OH layers on a range of ZnO surfaces using x-ray photoemission spectroscopy (XPS).^{33–36} These experimental observations have been accompanied by a number of first-principles density functional theory (DFT) studies that address the stability of various reconstruction geometries and adsorbate coverages. In the case of the Zn-polar face, Kresse *et al.*⁶ and Valtiner *et al.*^{10,27} have published phase diagrams that show a competition between triangular pit/terrace reconstructions and adsorbed OH overlayers with up to half-monolayer (1×2)-OH coverages. Wahl *et al.*³⁷ have produced similar phase diagrams for the O-polar face in which hexagonal honeycomblike reconstructions compete with hydroxylated surfaces with up to half-monolayer (1×2)-H coverages. Interestingly, while half-monolayer OH (H) overlayers on the Zn-polar (O-polar) faces satisfy the ECR and result in fully compensated semiconducting surfaces, experimental studies in both ambient and ultrahigh vacuum (UHV) conditions provide evidence for monolayer (1×1) OH (H) coverages and metallic (i.e., electron-accumulated) surfaces.^{33,38–40}

In this paper, we use a powerful combination of tunable photon energy synchrotron XPS and laboratory-based

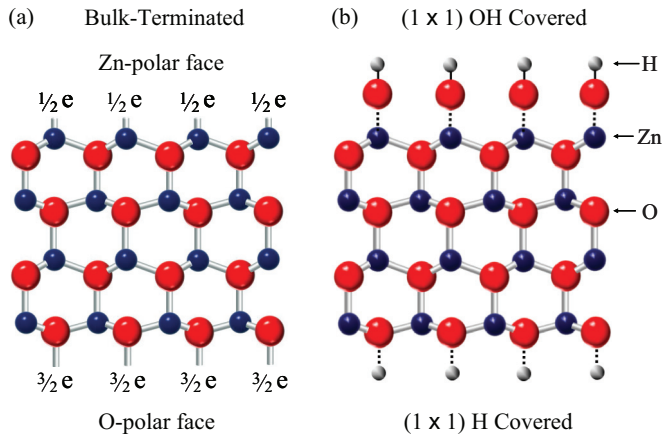


FIG. 1. (Color online) (a) Bulk ZnO termination and (b) the (1×1) hydroxyl termination of the Zn-polar (0001) and O-polar ($000\bar{1}$) faces of ZnO.

real-time *in situ* XPS to investigate the link between the surface chemistry and electronic nature of the polar ZnO surfaces. Using this approach, we have identified significant polarity-related differences in the thermal stability of the hydroxyl termination and the associated electron accumulation layers on the Zn-polar and O-polar faces. These differences have important implications for the fabrication of ohmic and rectifying metal contacts, heterostructure junctions, and homoepitaxial growth.

II. EXPERIMENTAL

A. Synchrotron radiation XPS

Core level and valence band (VB) XPS spectra were taken from the polar faces of ZnO single crystals following *in situ* heat treatments and subsequent H_2O/H_2 dosing at the soft x-ray beamline of the Australian Synchrotron, Melbourne. Photoemission spectra were collected using a Specs Phoibos 150 hemispherical electron energy analyzer with the detector axis arranged in the direction normal to the sample surface. All measurements were made without the use of an electron flood gun. Zn-polar and O-polar face samples ($5 \times 5 \times 0.5 \text{ mm}^3$) were cut from the same double-sided polished hydrothermally grown *c* axis ZnO single-crystal wafers obtained from Tokyo Denpa Co. Ltd. (Japan).⁴¹ Low-resistivity ($0.2 \Omega \text{ cm}$) wafers grown in the $-c$ direction were selected to avoid sample charging issues, the absence of which was confirmed by varying the incident photon flux.

All samples were cleaned using simple organic solvents (acetone, methanol, isopropyl alcohol, and N_2 gas drying) and then carefully attached to the sample holder using tantalum foil to ensure optimal thermal and electrical contact. Heat treatments (~ 15 -min duration) at temperatures from 150 – $750 \text{ }^\circ\text{C}$ and H_2O/H_2 dosing experiments were performed in a separate preparation chamber (nominal base pressure $\sim 5 \times 10^{-10}$ mbar) before being transferred to the UHV analyzer chamber (base pressure $\sim 1 \times 10^{-10}$ mbar), where XPS measurements were carried out in dark conditions at room temperature (RT). Low-energy electron diffraction (LEED) measurements were also performed in the preparation chamber to check for any surface

reconstruction after heat treatment and H_2O/H_2 dosing. The incident x-ray photon energy ($h\nu$) was varied for different scans to achieve optimum surface sensitivity: O $1s$ core level spectra were collected at $h\nu = 680 \text{ eV}$ to quantify the surface hydroxyl coverage, while VB spectra were collected at $h\nu = 150 \text{ eV}$ to maintain a similar photoelectron kinetic energy (of $\sim 150 \text{ eV}$) and similar escape depth. Survey spectra ($h\nu = 1486.6 \text{ eV}$) were also collected to allow comparisons with laboratory-based x-ray spectrometers. The binding energy (BE) scale of each scan was calibrated using the Au $4f$ core level doublet and the Fermi edge of a sputter-cleaned Au reference foil. The O $1s$ spectra were fitted using pseudo-Voigt functions on a Shirley background to extract the surface OH contribution with the full width at half maximum and the energetic separation of the components constrained. The H (OH) monolayer coverage on the O-polar (Zn-polar) surfaces was estimated from the relative peak areas of the fitted O $1s$ components using a Lambert-Beer absorption law approximation.^{42,43} The VB spectra were used to investigate changes in the near-surface band bending, following heat treatment and H_2O/H_2 dosing. Since the samples were carefully grounded to the spectrometer, the zero of the BE scale can be directly referenced to the Fermi level of the sample. The energetic position of the VB maximum in the near-surface region can then be determined from the low BE edge of the VB spectra, using the approach of Chambers *et al.*^{19,44}

B. Real-time *in situ* XPS

Real-time *in situ* XPS measurements were carried out while heat treating the polar surfaces of the same hydrothermally grown *c* axis ZnO wafers as in Sec. IIA using a fast acquisition system at Aberystwyth University specifically designed to study the kinetics of surface and interface formation. These experiments were performed in an UHV system (nominal base pressure $\sim 5 \times 10^{-10}$ mbar) using a Mg K_α ($h\nu = 1253.6 \text{ eV}$) x-ray source in conjunction with a Specs Phoibos 100 hemispherical electron analyzer with multichannel electron detection. *Ex situ* sample cleaning was carried out using the same organic solvent procedure as before. The cleaned samples were mounted onto a molybdenum sample holder that was then attached to an *in situ* graphite and boron nitride heater. The temperature was measured using a thermocouple bolted to the front of the heater faceplate close to the sample holder. After loading, the samples were *in situ* cleaned using a stable flux of plasma-generated atomic oxygen that efficiently removed the adventitious carbon contamination from the sample surface without significantly affecting the surface hydroxyl coverage. After plasma cleaning, the samples were briefly heated to $130 \text{ }^\circ\text{C}$ to remove excess adsorbed oxygen from the surface. Survey spectra were recorded in conventional scanning mode to confirm the surface composition and to calibrate the energy scales. The spectra were not affected by surface charging as there was no shift in peak position for different values of incident x-ray flux intensity.

Zn $2p_{3/2}$ and O $1s$ core level spectra were continually recorded in snapshot mode at 1 Hz, while heating O-polar and Zn-polar face samples from RT to $700 \text{ }^\circ\text{C}$. Each snapshot spectrum was fitted using a pseudo-Voigt function, and the BE of the extracted peak maxima was used to monitor shifts in the near-surface band bending of each sample during heat

treatment. Other examples of the use of snapshot core level photoemission spectra to monitor changes in surface band bending on semiconductor surfaces are described elsewhere.^{45,46} In addition, LEED measurements were also carried out in 50 °C steps from RT to the highest heating temperatures.

III. RESULTS

A. Synchrotron radiation XPS

Figure 2 shows typical O 1s core level spectra, VB spectra, and extracted energy band diagrams for the O-polar face after each of the following consecutive treatments: (a) as-loaded sample, (b) 15-min heating at 750 °C, and (c) 10000 L (Langmuir) H₂O dosing at RT. The dominant emission in the O 1s spectra [Figs. 2(a)–2(c)] is due to bulk oxygen, while the higher BE component (shifted to higher BE by 1.4 eV) is commonly attributed to surface hydroxyl groups.^{33–36} A third component at 533.8 eV, present in the as-loaded sample and after H₂O dosing, is associated with molecular water either on

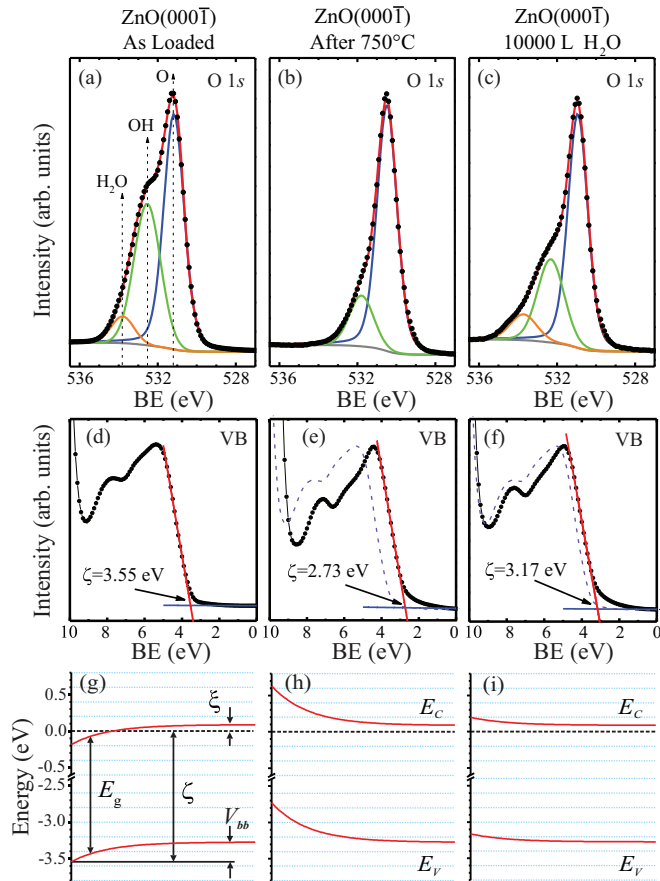


FIG. 2. (Color online) (a)–(c) O 1s core level XPS spectra taken using synchrotron radiation of $h\nu = 680$ eV on the O-polar face of single-crystal ZnO. Dots represent measured data points, and full lines represent fitted pseudo-Voigt functions of the bulk oxygen, surface hydroxyl, and surface water components on a Shirley background; (d)–(f) VB XPS spectra taken at $h\nu = 150$ eV showing the band bending parameter ζ obtained by extrapolating the low BE edge (red line) to the instrument background (blue line); (g)–(i) band bending schematic diagrams of the O-polar face after each treatment.

the crystal surface or on top of the surface hydroxyl groups.³⁸ It is clear from Fig. 2 that heat treatment at 750 °C causes a significant reduction in the surface OH component, which is partially recoverable on H₂O dosing.

The corresponding VB spectra taken during the same treatment sequence is shown in Figs. 2(d)–2(f). In each case, the energetic distance $\zeta = E_V - E_F$ between the VB maximum (E_V) and Fermi level (E_F) in the near-surface region was determined by extrapolating a linear fit of the low BE edge of the VB spectrum to a line fitted to the instrument background.^{19,44} The near-surface band bending (V_{bb}) was then obtained from $V_{bb} = E_g - \zeta - \xi$, where $\xi = (kT/q)\ln(N_C/n)$ is the energy difference between E_F and the conduction band minimum (E_C) in the bulk of the sample (n is the bulk carrier concentration $\sim 2 \times 10^{17}$ cm⁻³ and N_C is the conduction band effective density of states = 2.94×10^{18} cm⁻³ for ZnO). Negative values of V_{bb} correspond to downward surface band bending and electron accumulation, while positive values of V_{bb} are associated with upward band bending and the presence of a surface depletion region. The values of V_{bb} , ζ , and ξ were used to construct energy band diagrams for each of the treatment conditions, as shown in Figs. 2(g)–2(i). These show that the downward band bending on the as-loaded O-polar face was replaced by upward band bending following a simple 750 °C UHV heat treatment and that the reduced hydroxyl component appears to be associated with a change in the electronic nature of O-polar face from electron accumulation to carrier depletion. Subsequent dosing of this semiconducting (depleted) O-polar surface with 10000 L H₂O caused a partial recovery of the hydroxyl coverage, and at the same time, the upward band bending was significantly reduced to almost flat band conditions.

Figure 3 shows the equivalent measurements taken from the Zn-polar face in response to the same treatment sequence. Some significant differences are immediately apparent compared to the O-polar face: (i) the reduction in the surface hydroxyl component is noticeably smaller after an identical heat treatment, (ii) the energetic shift of the low BE edge of the VB spectrum is much smaller, and (iii) the downward band bending is not completely removed by the 750 °C heat treatment, indicating that the Zn-polar face remains in a state of electron accumulation.

To further investigate the relationship between hydroxyl termination and surface band bending, additional XPS measurements were taken on O-polar and Zn-polar samples after (i) heat treatment at increasing temperatures from 150–750 °C in 100 °C steps, (ii) after H₂O exposure of 750 °C heat-treated samples at increasing doses from 10 to 10000 L at RT, and (iii) after H₂ exposure of 750 °C heat treated samples at increasing doses from 10 to 1000 L at RT. The results of these experiments are shown in Fig. 4, which gives the relative peak areas of the OH and H₂O components (A_{OH} and A_{H_2O} , respectively) of the O 1s spectra and the surface band bending (V_{bb}) after each treatment. Significantly, these values of A_{OH} , A_{H_2O} , and V_{bb} were remarkably stable for samples in the UHV analyzer chamber ($\sim 1 \times 10^{-10}$ mbar), remaining unchanged for at least 8 h.

Figure 4 highlights significant differences in the response of the O-polar and Zn-polar faces to heat treatment and H₂O/H₂ dosing: For the O-polar face, there seems to be an inverse

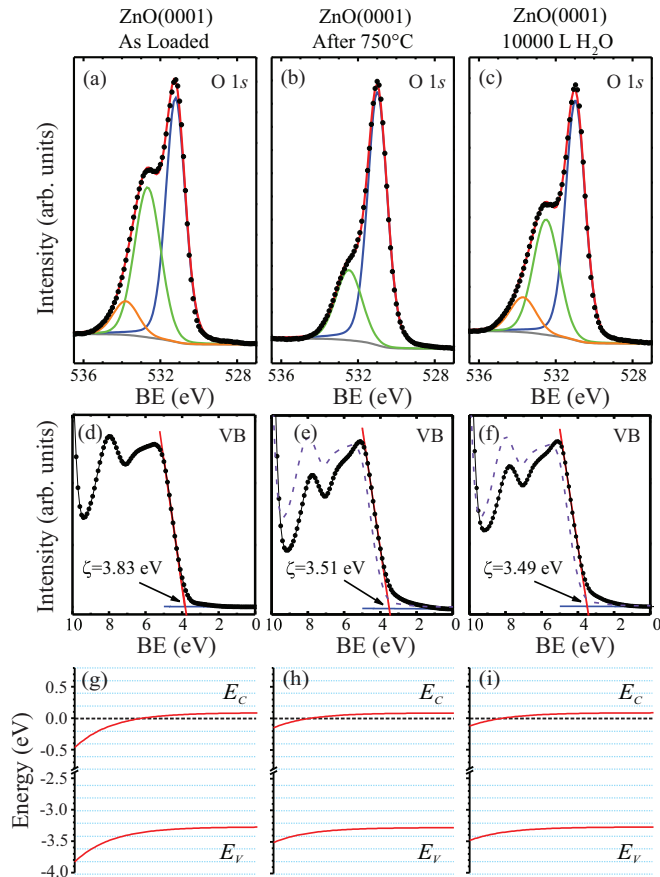


FIG. 3. (Color online) (a)–(c) O 1s core level spectra ($h\nu = 680$ eV), (d)–(f) VB spectra ($h\nu = 150$ eV), and (g)–(i) band bending diagrams for the Zn-polar face of single-crystal ZnO (measurements were taken and analyzed in an identical fashion to those on the O-polar face shown in Fig. 2).

relationship between the relative area of the OH component (A_{OH}) and the surface band bending V_{bb} . Furthermore, V_{bb} could be positively shifted by as much as 0.8 eV (nearly 1/4 of E_g) by heat treating up to 750 °C. The upward (positive) shift in V_{bb} could be gradually reversed by applying an increasing H₂O dose, while V_{bb} could be completely reset by briefly venting the sample to atmosphere. Remarkably, the near-surface region could be continually cycled between downward band bending (negative V_{bb}) and upward band bending (positive V_{bb}) by repeated applications of 750 °C heating and atmospheric exposure. At the same time, A_{OH} cycled between ~ 40 and $\sim 20\%$, respectively. Dosing the 750 °C heat-treated O-polar face with H₂ gas resulted in a similar but smaller negative shift in V_{bb} to that observed with H₂O dosing.

For the Zn-polar face, the downward band bending was consistently stronger and more resistant to heat treatment than on the O-polar face. The reduction of the OH component on heating was also smaller, and there appears to be a much weaker relationship between A_{OH} and V_{bb} (Fig. 4). After heating to 750 °C, the upward shift in V_{bb} was less than 0.4 eV, with most of this change occurring between 650 and 750 °C. This was insufficient to completely reverse the downward band bending on this face, with V_{bb} remaining negative. V_{bb} was then

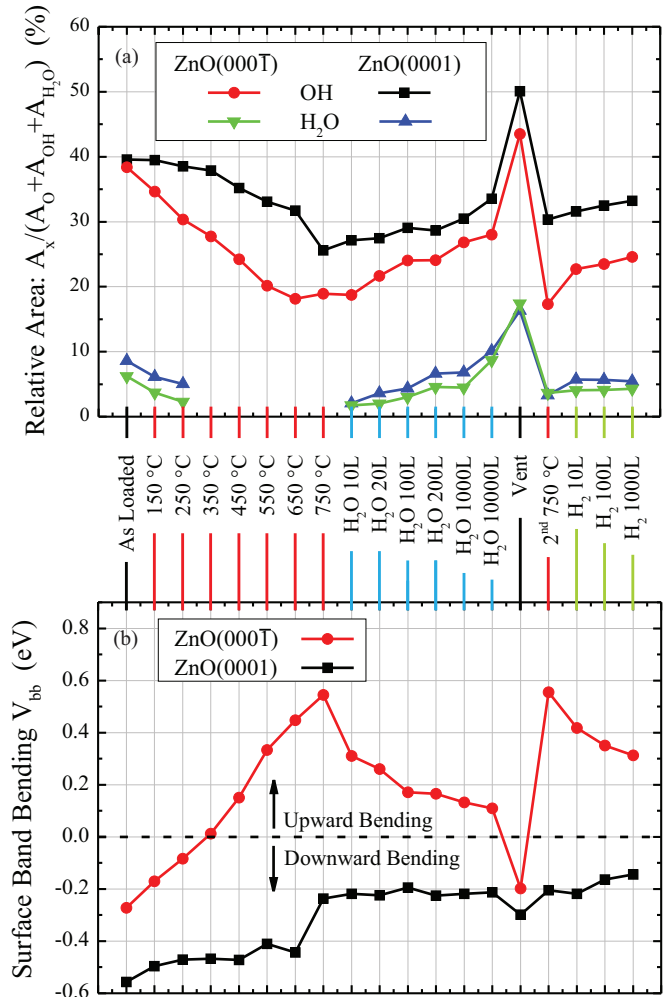


FIG. 4. (Color online) (a) Relative peak area of the OH and H₂O components (i.e., A_{OH} and A_{H_2O}) of the O 1s spectra taken from the O-polar and Zn-polar faces of single-crystal ZnO following different UHV heat treatments and subsequent H₂O/H₂ dosing and (b) the surface band bending V_{bb} extracted from the corresponding VB spectra. The horizontal dashed line represents flat near-surface bands.

unchanged after subsequent H₂O dosing at 10 to 10000 L, and atmospheric venting resulted in a small downward shift of only 0.1 eV. The inability of H₂O dosing or atmospheric exposure to reset V_{bb} on the Zn-polar face suggests that the 750 °C heat treatment caused a more permanent change to the surface structure than on the O-polar face.

Heating beyond 750 °C produced no significant further changes in V_{bb} on either the O-polar or Zn-polar face. However, after heating at 900 °C, gap states were observed in the VB spectra of both polar faces (see Fig. 5, vertical arrow). Similar states have also been observed following the *in situ* cleaving of bulk ZnO crystals⁴⁷ and also in recent DFT calculations that considered the effect of Zn vacancies on the VB density of states of ZnO.¹² At the same time, sodium, potassium, and calcium peaks were observed in the $h\nu = 1486.6$ eV survey spectra. Hydrothermal ZnO contains significant levels of group I impurities that are known to diffuse towards the surface at elevated temperatures, along with other common impurities, such as aluminum and gallium.⁴⁸ These observations suggest

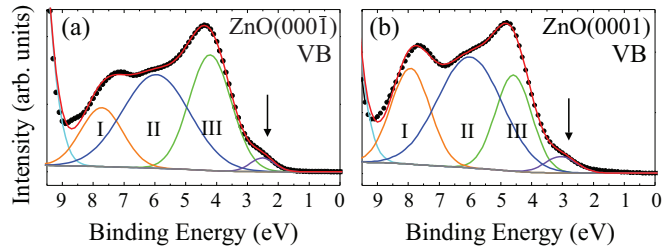


FIG. 5. (Color online) VB XPS spectra taken from (a) the O-polar face and (b) the Zn-polar face of single-crystal ZnO after 15 min of heating at 900 °C. Dots represent measured data points, and full lines represent pure Gaussian fits to VB peaks I, II, and III (Ref. 47). The vertical arrow indicates electronic states with subband-gap binding energies.

that UHV heating at temperatures above 800 °C resulted in permanent changes, such as surface decomposition-sublimation and the surface aggregation of impurities.

B. Real-time *in situ* XPS

Real-time changes in the electronic nature of the polar ZnO surfaces were directly monitored during heat treatment between RT and ~ 700 °C by recording Zn $2p_{3/2}$ and O $1s$ core level spectra at 1-sec intervals in snapshot mode at a pass energy of 100 eV using Mg K_{α} (1253.6-eV) radiation. The Zn $2p_{3/2}$ core level spectra provided the highest signal-to-noise ratio. Since the Zn $2p_{3/2}$, O $1s$, and VB spectra showed almost identical BE shifts, the position of the Zn $2p_{3/2}$ peak maxima was used to provide a direct indication of the surface band bending V_{bb} of the sample, i.e., shifts to lower BE were associated with more positive values of V_{bb} and either a reduction in downward band bending or an increase in upward band bending. No BE shifts were observed on varying the intensity of the incident x rays, ruling out the influence of sample charging. Furthermore, the peak positions of the as-received samples prior to heat treatment were similar to those observed in the synchrotron experiment (Sec. III A).

Figure 6 shows the time evolution of the Zn $2p_{3/2}$ core level spectra taken from the O-polar face during a 70-min heating and cooling cycle. The programmed temperature cycle and the associated variations in chamber pressure are shown in Fig. 6(b). The solid white line in Fig. 6(a) tracks the BE position of the peak maxima of a pseudo-Voigt function fitted to each Zn $2p_{3/2}$ snapshot spectrum, while the horizontal dashed white line indicates the time at which the highest temperature was reached and the sample began to cool.

After an initial stable period, the Zn $2p_{3/2}$ peak maxima steadily shifted to lower BE, as the O-polar face was heated to 640 °C. This corresponds to a significant upward shift of ~ 0.8 eV in surface band bending (V_{bb}) similar to that observed in the synchrotron experiment. Figure 6(a) also shows a slow partial recovery to higher BE as the sample cooled that was not observed previously and is most probably due to the rehydroxylation of the O-polar face from the higher H₂O/hydrogen partial pressures in this UHV system, especially during the heating cycles.

Figure 7 shows the equivalent real-time heating measurements carried out on the Zn-polar face. This shows a

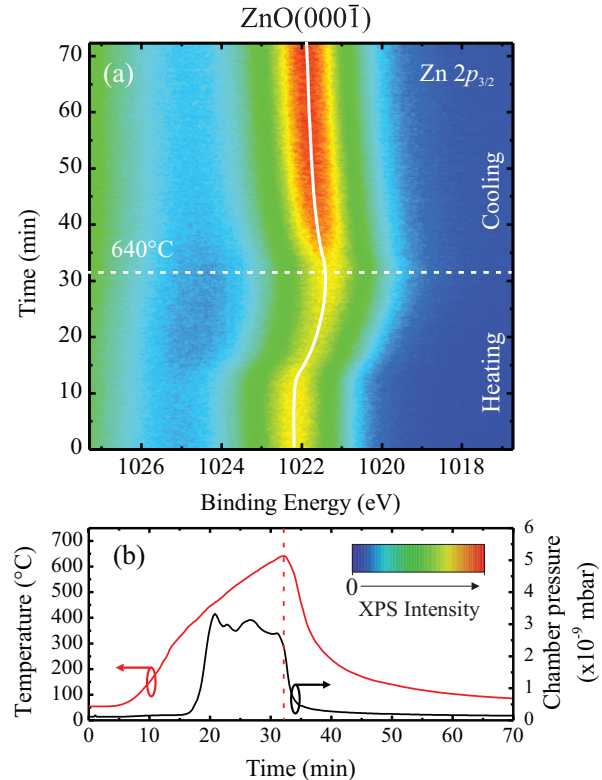


FIG. 6. (Color online) (a) Projection view of the real-time evolution of the Zn $2p_{3/2}$ core level emission on the O-polar face during *in situ* heating and (b) the sample temperature and chamber pressure versus time [note: a negative BE shift corresponds to a positive (upward) shift in V_{bb}].

significantly smaller shift (~ 0.4 eV) of the Zn $2p_{3/2}$ peak to lower BE during heating compared to that observed for the O-polar face. This is consistent with the much smaller upward shift in band bending observed after heat treatment in the synchrotron experiment. In contrast to the O-polar face, the BE shift was completely reversed within the 70-min heating-cooling cycle.

The results from Figs. 6 and 7 were used to construct plots of real-time BE shift versus temperature for both the Zn-polar and O-polar face (see Fig. 8). The BE shift on the Zn-polar face [Fig. 8(a)] was approximately symmetrical for both heating and cooling, returning to the same BE value at RT. For the O-polar face [Fig. 8(b)], only a small negative BE shift with temperature was observed up to a threshold of ~ 280 °C, after which the rate of BE shift increased by a factor of ~ 20 , eventually reaching a shift of -0.8 eV at 640 °C. Subsequent cooling resulted in a hysteresislike recovery to the initial BE value, with a significant part of this recovery occurring close to RT over the course of several hours (data not shown in Fig. 8). This is attributed to the slow rehydroxylation of the O-polar surface from background water vapor-hydrogen in this UHV system. Figure 8(c) shows a second heating cycle on the same O-polar face sample to a temperature of 400 °C during which the same behavior was observed. Further experiments on other O-polar face samples consistently showed similar hysteresis effects. This suggests that in a given UHV system, there is a processing window in which semiconducting (depleted)

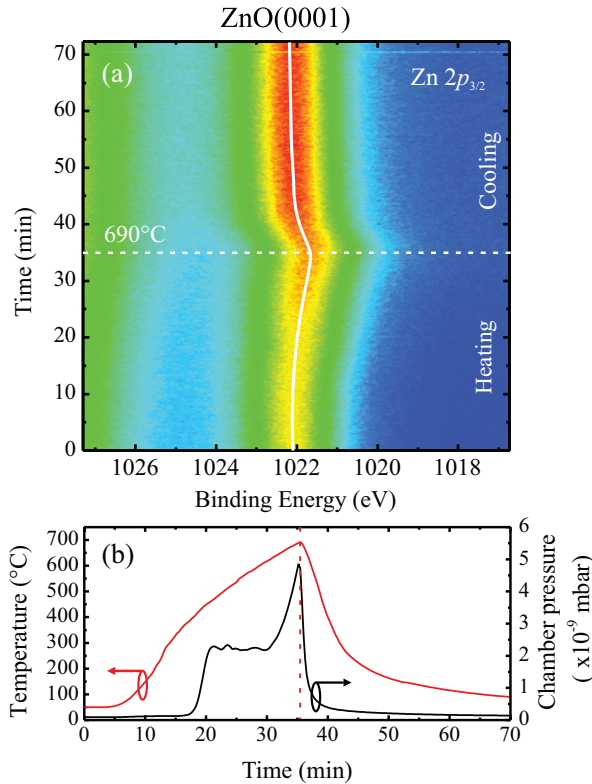


FIG. 7. (Color online) (a) Projection view of the real-time evolution of the Zn $2p_{3/2}$ core level emission on the Zn-polar face during *in situ* heating and (b) the sample temperature and chamber pressure versus time.

O-polar surfaces can be prepared and maintained for the fabrication of devices such as heterojunctions and Schottky contacts.

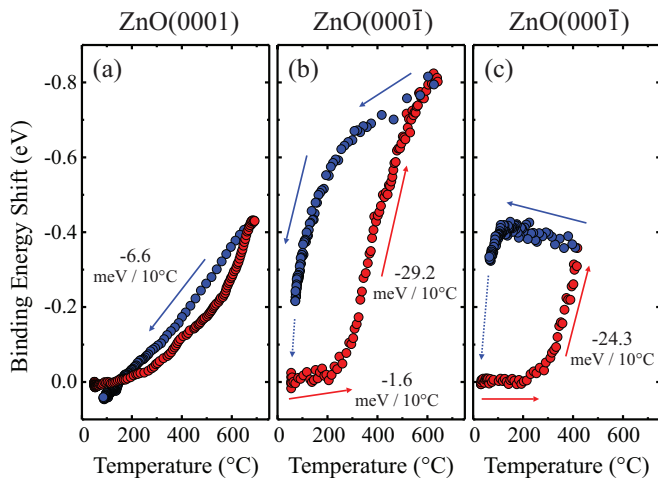


FIG. 8. (Color online) Binding energy shift in the position of the Zn $2p_{3/2}$ photoemission peak recorded (in real time) from (a) the Zn-polar face and (b) the O-polar face versus temperature during UHV heating (red circles) and cooling (blue circles). Figure 8(c) shows the results of a subsequent heating cycle on the same O-polar face sample.

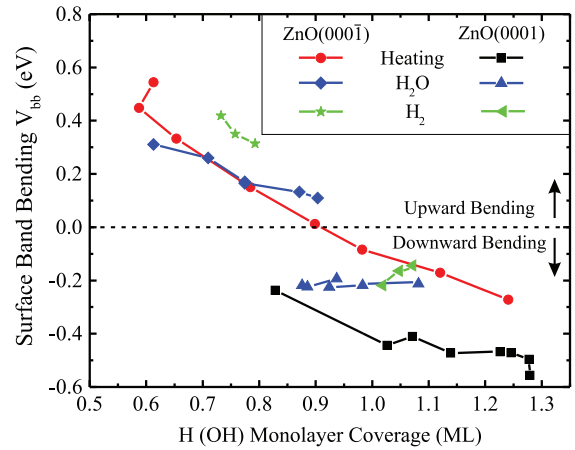


FIG. 9. (Color online) Surface band bending (V_{bb}) versus H(OH) monolayer coverage on the O-polar (Zn-polar) face of single-crystal ZnO, extracted from synchrotron XPS following different UHV heat treatments (up to 750 °C) and subsequent H_2O/H_2 dosing.

IV. DISCUSSION

Significant differences in the stability of the hydroxyl termination on the O-polar and Zn-polar faces of ZnO with respect to UHV heating were observed using surface-sensitive synchrotron XPS measurements. This is perhaps not surprising given that changes in the hydroxyl termination on the O-polar face involve the gain or loss of H atoms from the bulk-terminated surface, while on the Zn-polar face, OH groups are involved.

Figure 9 shows the relationship between the H(OH) coverage and the surface band bending V_{bb} for the O-polar (Zn-polar) faces, extracted from the synchrotron data shown in Fig. 4. In the case of the O-polar face, there appears to be a strong correlation between H coverage and V_{bb} , with decreasing H coverage associated with increasing V_{bb} (i.e., upward shifts in band bending). Furthermore, V_{bb} becomes zero at an H coverage of approximately 0.9 ML corresponding to flat near-surface bands. For H coverages less than this, the near-surface bands bend upwards resulting in carrier depletion and a metallic to semiconductorlike transition in the electronic nature of the surface. The lowest H coverage obtained using simple UHV heating up to 750 °C was approximately 0.59 ML, close to the 0.5 ML coverage predicted by first-principles DFT phase diagrams for unreconstructed semiconducting surfaces obeying the ECR.^{6,10,27,37}

LEED measurements taken from the O-polar face for each of the H coverages shown in Fig. 9 showed no change in the unreconstructed (1×1) pattern, with sixfold symmetry, observed in the as-loaded sample. This is consistent with the observations of Kunat *et al.*³⁵ that only clean H-free O-polar surfaces reconstruct (into an ordered (1×3) oxygen vacancy structure) and that H-saturated surfaces are always unreconstructed. Here, we can extend the unreconstructed O-polar face to H coverages approaching 0.5 ML. Clean (H-free) O-polar surfaces are difficult to prepare requiring a number of Ar^+ sputtering cycles in UHV, followed by annealing in an oxygen ambient to repair the sputter-induced damage.^{15,35} Here, we find that semiconducting (depleted)

O-polar surfaces with H coverages approaching 0.5 ML are much easier to prepare, requiring only a simple UHV heat treatment.

Figures 4 and 9 also show that semiconducting (depleted) O-polar surfaces are not stable with respect to the presence of H_2O or H_2 , both of which cause an increase in H coverage and a downward shift in band bending. However, complete rehydroxylation of the O-polar face and a recovery of the as-loaded downward band bending could not be achieved with *in situ* H_2O dosing up to 10 000 L and required exposure of the O-polar face to atmosphere. This slow rehydroxylation is in contrast to the high reactivity of the clean, reconstructed (1×3) O-polar surface towards H_2O .^{35,38} This can be explained with models of H_2O dissociation that require the presence of oxygen vacancies.^{49,50} These will be present in much higher densities on the clean, reconstructed (1×3) O-polar face which is characterized by one O-atom vacancy per unit cell,⁴⁹ compared with the fully occupied (1×1) unreconstructed O-polar surfaces observed here.

In the case of the Zn-polar face, the relationship between OH coverage and V_{bb} is not as convincing. The surface band bending V_{bb} is significantly more negative on the Zn-polar face and appears almost constant for OH coverages greater than 1 ML. The lowest OH coverage achieved using heat treatment up to 750 °C was ~ 0.8 ML for which V_{bb} was still negative (i.e., -0.2 eV), indicating that the bands on the Zn-polar face were still bent downward. Surprisingly, no change in V_{bb} was evident on subsequent *in situ* H_2O dosing up to 10 000 L even though the OH coverage increased to more than 1 ML.

As-loaded polar ZnO surfaces and those exposed to atmospheric conditions have hydroxyl terminations in excess of 1 ML (Figs. 4 and 9), significantly higher than the 0.5 ML coverage predicted by first-principles studies (and the ECR) for stable semiconducting surfaces. At the same time, these surfaces are characterized by downward band bending consistent with the presence of electron accumulation layers.^{14,15} Calzolari *et al.*¹² recently showed using DFT calculations that saturation H (OH) coverages on the O-polar (Zn-polar) face of ZnO induce a physical semiconductor-to-metal transition, with the extra H atoms acting as surface n donors. It has also been proposed that H atoms donate ~ 0.5 electrons to each surface oxygen atom on both the OH-terminated O-polar and Zn-polar ZnO surfaces.^{33,51} Furthermore, the unusual position of the CNL of ZnO above the conduction band minimum is known to favor the formation of donorlike surface states and promote an electrically active donor role for hydrogen.^{19–21} In light of the behavior shown in Fig. 9, it appears that hydrogen in the OH-termination of the polar surfaces of ZnO provides a source of donorlike surface states for the observed surface electron accumulation layers, although this link is less straightforward in the case of the Zn-polar face.

One outstanding question is whether hydrogen in the subsurface region plays a role in the downward band bending and electron accumulation at ZnO surfaces. Traeger *et al.*⁵² quantified the hydrogen concentration profile in hydrothermal ZnO single crystals using ^{15}N nuclear reaction analysis and reported significantly higher hydrogen concentrations in the subsurface region compared to the bulk. In addition, part of this subsurface hydrogen was found to be less strongly

bound and could be removed by heating to 550 °C and then subsequently reloaded on exposure to atomic hydrogen. Hydrogen incorporates into the ZnO lattice at a variety of bonding sites that anneal out at different temperatures: These include bond-centered hydrogen (~ 190 °C), hydrogen bound at oxygen vacancies (~ 500 °C), OH- Li_{Zn} complexes (650–1200 °C), and so-called hidden molecular hydrogen.^{53–55} Here, we have observed that the electron accumulation layer can be easily reestablished on semiconducting (depleted) O-polar ZnO surfaces by simple atmospheric exposure. Therefore, in order for subsurface hydrogen to be involved, some mechanism would be required that increases the subsurface hydrogen concentration on exposure to atmospheric water vapor. In the case of rutile TiO_2 , it has been proposed that H atoms from the hydroxylated $\text{TiO}_2(110)$ surface are able to migrate to subsurface sites with a relatively low activation energy,^{56,57} while water dissociation on the SrO-terminated face of $\text{SrTiO}_3(001)$ leads to hydroxyl pairs in the entire submonolayer regime.⁵⁸

Although it has long been known that surface hydroxyls can stabilize polar oxide surfaces, such as $\text{Al}_2\text{O}_3(0001)$, $\text{Fe}_2\text{O}_3(0001)$, and the (111) surface of rocksalt oxides NiO, CoO, and MgO,^{26,59–61} they have only been directly associated with surface electron accumulation in the case of ZnO. For other oxide semiconductors with strong near-surface downward band bending, i.e., In_2O_3 , CdO, and SnO_2 , the identity of the donors that provide the free electrons within their surface accumulation layers is still the subject of debate. Hydrogen is known to be a shallow donor in these other oxide semiconductors,^{20,22,62} however, surface oxygen vacancies acting as doubly ionized shallow donors have recently been proposed as the microscopic origin of surface electron accumulation in In_2O_3 .^{63,64}

V. SUMMARY AND CONCLUSIONS

Surface-sensitive synchrotron x-ray photoemission spectroscopy (XPS) and real-time *in situ* XPS revealed significant differences in the thermal stability of the hydroxyl termination and associated downward band bending on the polar surfaces of ZnO. The band bending on the O-polar face could be reversibly switched over a range of ~ 0.8 eV by adjusting the H coverage using simple UHV heat treatments, dosing with H_2O or H_2 and atmospheric exposure. A strong relationship was found between H coverage (in ML) and near-surface band bending on the O-polar face, with a transition from downward to upward band bending occurring at coverages of ~ 0.9 ML. Semiconducting (i.e., depleted) O-polar surfaces with H coverages approaching the 0.5-ML level predicted by first-principles calculations could be prepared using a simple UHV heat treatment at 750 °C. Interestingly, the real-time XPS measurements indicated a distinct threshold temperature at ~ 280 °C on the O-polar face after which there was a dramatic increase in the rate of upward band bending with temperature.

A significant difference in the thermal stability of the OH termination between the two polar surfaces was observed with a significantly lower rate of thermal desorption on the Zn-polar face. The downward band bending on the Zn-polar face was remarkably resilient to heating and depleted surfaces could not be created by heat treatment alone.

Under normal atmospheric and device preparation conditions the hydroxyl termination on the O-polar and Zn-polar faces of ZnO will significantly exceed the 0.5-ML coverage predicted for semiconducting ZnO surfaces, and consequently these surfaces are likely to be metallic in nature. However, the O-polar face can be easily switched between electron accumulation and depletion by simple UHV heat treatment with important implications for the fabrication of ohmic and rectifying metal contacts, heterostructure junctions, and homoepitaxial growth.

ACKNOWLEDGMENTS

This work was directly supported by the New Zealand Marsden Fund under Grant No. UOC0909 and by the

MacDiarmid Institute for Advanced Materials and Nanotechnology. The real-time measurements were supported by the United Kingdom Engineering and Physical Sciences Research Council and the Higher Education Funding Council for Wales. M.W.A. is a current recipient of a Royal Society of New Zealand Rutherford Discovery Fellowship, and D.A.E. received a University of Canterbury Erskine Fellowship during the course of this work. We acknowledge beam time and the assistance of B. Cowie, L. Thomsen, and A. Tadich at the Australian Synchrotron, Victoria, Australia. We are also grateful for useful discussions with D. Y. Zemlyanov (Purdue University), J. B. Metson (University of Auckland), T. D. Veal (University of Liverpool), C. F. McConville (University of Warwick), R. Clarke (University of Michigan), S. M. Durbin (University of Western Michigan), and R. J. Reeves (University of Canterbury).

*martin.allen@canterbury.ac.nz

- ¹C. Klingshirn, *Phys. Status Solidi B* **244**, 3027 (2007).
- ²U. Özgür, D. Hofstetter, and H. Morkoç, *Proc. IEEE* **98**, 1255 (2010).
- ³S. E. Chamberlin, C. J. Hirschmugl, S. T. King, H. C. Poon, and D. K. Saldin, *Phys. Rev. B* **84**, 075437 (2011).
- ⁴M. H. Du, S. B. Zhang, J. E. Northrup, and S. C. Erwin, *Phys. Rev. B* **78**, 155424 (2008).
- ⁵O. Dulub, U. Diebold, and G. Kresse, *Phys. Rev. Lett.* **90**, 016102 (2003).
- ⁶G. Kresse, O. Dulub, and U. Diebold, *Phys. Rev. B* **68**, 245409 (2003).
- ⁷J. V. Lauritsen, S. Porsgaard, M. K. Rasmussen, M. C. R. Jensen, R. Bechstein, K. Meinander, B. S. Clausen, S. Helveg, R. Wahl, G. Kresse, and F. Besenbacher, *ACS Nano* **5**, 5987 (2011).
- ⁸B. Meyer and D. Marx, *Phys. Rev. B* **67**, 035403 (2003).
- ⁹S. Torbrugge, F. Ostendorf, and M. Reichling, *J. Phys. Chem. C* **113**, 4909 (2009).
- ¹⁰M. Valtiner, M. Todorova, G. Grundmeier, and J. Neugebauer, *Phys. Rev. Lett.* **103**, 065502 (2009).
- ¹¹A. Wander, F. Schedin, P. Steadman, A. Norris, R. McGrath, T. S. Turner, G. Thornton, and N. M. Harrison, *Phys. Rev. Lett.* **86**, 3811 (2001).
- ¹²A. Calzolari, M. Bazzani, and A. Catellani, *Surf. Sci.* **607**, 181 (2013).
- ¹³J. Lahiri, S. Senanayake, and M. Batzill, *Phys. Rev. B* **78**, 155414 (2008).
- ¹⁴M. W. Allen, C. H. Swartz, T. H. Myers, T. D. Veal, C. F. McConville, and S. M. Durbin, *Phys. Rev. B* **81**, 075211 (2010).
- ¹⁵K. Ozawa and K. Mase, *Phys. Rev. B* **83**, 125406 (2011).
- ¹⁶L. F. J. Piper, A. R. H. Preston, A. Fedorov, S. W. Cho, A. DeMasi, and K. E. Smith, *Phys. Rev. B* **81**, 233305 (2010).
- ¹⁷O. Schmidt, P. Kiesel, D. Ehrentraut, T. Fukuda, and N. M. Johnson, *Appl. Phys. A* **88**, 71 (2007).
- ¹⁸A. Schleife, F. Fuchs, C. Rödl, J. Furthmüller, and F. Bechstedt, *Appl. Phys. Lett.* **94**, 012104 (2009).
- ¹⁹P. D. C. King, T. D. Veal, D. J. Payne, A. Bourlange, R. G. Egdell, and C. F. McConville, *Phys. Rev. Lett.* **101**, 116808 (2008).
- ²⁰P. D. C. King, R. L. Lichti, Y. G. Celebi, J. M. Gil, R. C. Vilão, H. V. Alberto, J. Piroto Duarte, D. J. Payne, R. G. Egdell, I. McKenzie, C. F. McConville, S. F. J. Cox, and T. D. Veal, *Phys. Rev. B* **80**, 081201(R) (2009).
- ²¹C. G. Van de Walle and J. Neugebauer, *Nature (London)* **423**, 626 (2003).
- ²²P. D. C. King, T. D. Veal, P. H. Jefferson, J. Zúñiga-Pérez, V. Muñoz-Sanjosé, and C. F. McConville, *Phys. Rev. B* **79**, 035203 (2009).
- ²³V. Avrutin, G. Cantwell, J. Z. Zhang, J. J. Song, D. J. Silversmith, and H. Morkoc, *Proc. IEEE* **98**, 1339 (2010).
- ²⁴C. Wöll, *Prog. Surf. Sci.* **82**, 55 (2007).
- ²⁵P. W. Tasker, *J. Phys. C* **12**, 4977 (1979).
- ²⁶J. Goniakowski, F. Finocchi, and C. Noguera, *Rep. Prog. Phys.* **71**, 016501 (2008).
- ²⁷M. Valtiner, M. Todorova, and J. Neugebauer, *Phys. Rev. B* **82**, 165418 (2010).
- ²⁸G. Heiland and P. Kunstmann, *Surf. Sci.* **13**, 72 (1969).
- ²⁹D. J. Chadi, *J. Vac. Sci. Technol. A* **5**, 834 (1987).
- ³⁰M. D. Pashley, *Phys. Rev. B* **40**, 10481 (1989).
- ³¹L. X. Zhang, E. G. Wang, Q. K. Xue, S. B. Zhang, and Z. Y. Zhang, *Phys. Rev. Lett.* **97**, 126103 (2006).
- ³²S. Pal, T. Jasper-Tönnies, M. Hack, and E. Pehlke, *Phys. Rev. B* **87**, 085445 (2013).
- ³³B. J. Coppa, C. C. Fulton, P. J. Hartlieb, R. F. Davis, B. J. Rodriguez, B. J. Shields, and R. J. Nemanich, *J. Appl. Phys.* **95**, 5856 (2004).
- ³⁴B. J. Coppa, C. C. Fulton, S. M. Kiesel, R. F. Davis, C. Pandarinath, J. E. Burnette, R. J. Nemanich, and D. J. Smith, *J. Appl. Phys.* **97**, 103517 (2005).
- ³⁵M. Kunat, S. G. Girol, T. Becker, U. Burghaus, and C. Wöll, *Phys. Rev. B* **66**, 081402 (2002).
- ³⁶M. W. Allen, D. Y. Zemlyanov, G. I. N. Waterhouse, J. B. Metson, T. D. Veal, C. F. McConville, and S. M. Durbin, *Appl. Phys. Lett.* **98**, 101906 (2011).
- ³⁷R. Wahl, J. V. Lauritsen, F. Besenbacher, and G. Kresse, *Phys. Rev. B* **87**, 085313 (2013).
- ³⁸M. Schiek, K. Al-Shamery, M. Kunat, F. Traeger, and C. Wöll, *Phys. Chem. Chem. Phys.* **8**, 1505 (2006).
- ³⁹C. M. Schlepütz, Y. Yang, N. S. Husseini, R. Heinhold, H-S. Kim, M. W. Allen, and S. M. Durbin, and R. Clarke, *J. Phys.: Condens. Matter* **24**, 095007 (2012).

- ⁴⁰M. Valtiner, S. Borodin, and G. Grundmeier, *Phys. Chem. Chem. Phys.* **9**, 2406 (2007).
- ⁴¹K. Maeda, M. Sato, I. Niikura, and T. Fukuda, *Semicond. Sci. Technol.* **20**, S49 (2005).
- ⁴²Y. Joseph, W. Ranke, and W. Weiss, *J. Phys. Chem. B* **104**, 3224 (2000).
- ⁴³A. Önsten, D. Stoltz, P. Palmgren, S. Yu, T. Claesson, M. Göthelid, and U. O. Karlsson, *Surf. Sci.* **608**, 31 (2013).
- ⁴⁴S. A. Chambers, T. Droubay, T. C. Kaspar, and M. Gutowski, *J. Vac. Sci. Technol. B* **22**, 2205 (2004).
- ⁴⁵D. A. Evans, O. R. Roberts, A. R. Vearey-Roberts, D. P. Langstaff, D. J. Twitchen, and M. Schwitters, *Appl. Phys. Lett.* **91**, 132114 (2007).
- ⁴⁶D. A. Evans, O. R. Roberts, A. R. Vearey-Roberts, G. T. Williams, A. C. Brieva, and D. P. Langstaff, *Appl. Phys. Lett.* **102**, 021605 (2013).
- ⁴⁷R. Heinhold and M. W. Allen, *J. Mater. Res.* **27**, 2214 (2012).
- ⁴⁸R. Heinhold, H.-S. Kim, F. Schmidt, H. von Wenckstern, M. Grundmann, R. J. Mendelsberg, R. J. Reeves, S. M. Durbin, and M. W. Allen, *Appl. Phys. Lett.* **101**, 062105 (2012).
- ⁴⁹M. Kunat, S. Gil Girol, U. Burghaus, and C. Wöll, *J. Phys. Chem. B* **107**, 14350 (2003).
- ⁵⁰H. Noei, H. Qiu, Y. Wang, E. Löffler, C. Wöll, and M. Muhler, *Phys. Chem. Chem. Phys.* **10**, 7092 (2008).
- ⁵¹V. E. Heinrich and P. A. Cox, *The Surface Science of Metal Oxides* (Cambridge University Press, Cambridge, 1994), p. 297.
- ⁵²F. Traeger, M. Kauer, C. Wöll, D. Rogalla, and H.-W. Becker, *Phys. Rev. B* **84**, 075462 (2011).
- ⁵³E. V. Lavrov, F. Herklotz, and J. Weber, *Phys. Rev. B* **79**, 165210 (2009).
- ⁵⁴K. M. Johansen, H. Haug, E. Lund, E. V. Monakhov, and B. G. Svensson, *Appl. Phys. Lett.* **97**, 211907 (2010).
- ⁵⁵M. H. Du and K. Biswas, *Phys. Rev. Lett.* **106**, 115502 (2011).
- ⁵⁶X.-L. Yin, M. Calatayud, H. Qiu, Y. Wang, A. Birkner, C. Minot, and C. Wöll, *Chem. Phys. Chem.* **9**, 253 (2008).
- ⁵⁷G. H. Enevoldsen, H. P. Pinto, A. S. Foster, M. C. R. Jensen, W. A. Hofer, B. Hammer, J. V. Lauritsen, and F. Besenbacher, *Phys. Rev. Lett.* **102**, 136103 (2009).
- ⁵⁸H. Guhl, W. Miller, and K. Reuter, *Phys. Rev. B* **81**, 155455 (2010).
- ⁵⁹M. A. Langel and M. H. Nassir, *J. Phys. Chem.* **99**, 4162 (1995).
- ⁶⁰D. Cappus, M. Hassel, E. Neuhaus, M. Heber, F. Rohr, and H.-J. Freund, *Surf. Sci.* **337**, 268 (1995).
- ⁶¹V. K. Lazarov, R. Plass, H.-C. Poon, D. K. Saldin, M. Weinert, S. A. Chambers, and M. Gajdardziska-Josifovska, *Phys. Rev. B* **71**, 115434 (2005).
- ⁶²S. Limpijumnong, P. Reunchan, A. Janotti, and C. G. Van de Walle, *Phys. Rev. B* **80**, 193202 (2009).
- ⁶³S. Lany, A. Zakutayev, T. O. Mason, J. F. Wager, K. R. Poepplmeier, J. D. Perkins, J. J. Berry, D. S. Ginley, and A. Zunger, *Phys. Rev. Lett.* **108**, 016802 (2012).
- ⁶⁴K. H. L. Zhang, R. G. Egdell, F. Offi, S. Iacobucci, L. Petaccia, S. Gorovikov, and P. D. C. King, *Phys. Rev. Lett.* **110**, 056803 (2013).